NOTES AND CORRESPONDENCE

Using Normalized Climatological Anomalies to Rank Synoptic-Scale Events Objectively

ROBERT E. HART

Department of Meteorology, The Pennsylvania State University, University Park, Pennsylvania

RICHARD H. GRUMM

National Weather Service, State College, Pennsylvania

14 January 2000 and 15 January 2001

ABSTRACT

A method for ranking synoptic-scale events objectively is presented. NCEP 12-h reanalysis fields from 1948 to 2000 are compared to a 30-yr (1961–90) reanalysis climatology. The rarity of an event is the number of standard deviations 1000–200-hPa height, temperature, wind, and moisture fields depart from this climatology. The top 20 synoptic-scale events from 1948 to 2000 for the eastern United States, southeast Canada, and adjacent coastal waters are presented. These events include the ''The Great Atlantic Low'' of 1956 (ranked 1st), the ''superstorm'' of 1993 (ranked 3d), the historic New England/Quebec ice storm of 1998 (ranked 5th), extratropical storm Hazel of 1954 (ranked 9th), a catastrophic Florida freeze and snow in 1977 (ranked 11th), and the great Northeast snowmelt and flood of 1996 (ranked 12th).

During the 53-yr analysis period, only 33 events had a total normalized anomaly (M_{TOTAL}) of 4 standard deviations or more. An M_{TOTAL} of 5 or more standard deviations has not been observed during the 53-yr period. An M_{TOTAL} of 3 or more was observed, on average, once or twice a month. October through January are the months when a rare anomaly ($M_{\text{TOTAL}} \geq 4$ standard deviations) is most likely, with April through September the least likely period. The 1960s and 1970s observed the fewest number of monthly top 10 events, with the 1950s, 1980s, and 1990s having the greatest number. A comparison of the evolution of M_{TOTAL} to various climate indices reveals that only 5% of the observed variance of M_{TOTAL} can be explained by ENSO, North Atlantic oscillations, or Pacific–North American indices. Therefore, extreme synoptic-scale departures from climatology occur regardless of the magnitude of conventional climate indices, a consequence of a necessary mismatch of temporal and spatial scale representation between the M_{TOTAL} and climate index measurements.

1. Introduction

Several methods have been developed to rank meteorological events in terms of severity, social impact, or economic impact. The Fujita scale (Fujita 1981) ranks tornadoes based upon wind damage patterns. The Saffir–Simpson scale ranks hurricanes based upon the maximum wind speed (Simpson 1974). Palmer (1965) developed a scale for measuring drought severity. Dolan and Davis developed a scale for ranking United States coastal storms based upon wave height and duration (Watson 1993).

Historically, the storms that are deemed the most significant are those that usually achieve the greatest media attention or impact the largest population centers (e.g., Kocin and Uccellini 1990). This subjectivity is compounded by preparedness issues. A winter storm of a given size or intensity usually has greater impact upon the population at lower latitudes than the same storm would at higher latitudes. Further, the observation network is biased toward the densely populated urban corridors and against rural and oceanic areas. Clearly, the ranking of meteorological phenomena within both the media and the meteorological community is subjective.

Accordingly, it is important to make the distinction between a purely meteorological event that is rare and a meteorological–sociological event that is rare. Not all rare synoptic-scale meteorological events attract significant media attention. Several impact scarcely or nonpopulated areas (70% of the earth's surface is water), or occur during the time of year when precipitation falls as liquid. It is possible that several of the most anomalous events of the past century have impacted completely unpopulated areas, and are greatly underrepresented in the literature. For example, The Queen Elizabeth II storm might not have become a classic case

Corresponding author address: Dr. Robert E. Hart, Department of Meteorology, The Pennsylvania State University, 503 Walker Building, University Park, PA 16802.
E-mail: hart@ems.psu.edu

TABLE 1. Pressure levels at which NCEP reanalysis data are available.

Level (hPa)	Height	Temperature	Wind	Specific humidity
1000	√	√	√	√
925	√	√	√	√
850	√	√	√	√
700	√	√	√	√
600	√	√	√	√
500	√	√	√	√
400	√	√	√	√
300	√	√	√	√
250	√	√	√	
200	√	√	√	

study (Anthes et al. 1983; Gyakum 1983a,b, 1991; Uccellini 1986) had it not struck the ship. However, since the most baroclinically active regions of the world (Sanders and Gyakum 1980; Hoskins and Valdes 1990) are located near populated coastal areas, it is likely that most (but not all) extreme events during the past century *have* been observed if not documented.

In this paper, a simple yet comprehensive method is proposed for *objectively* ranking synoptic-scale events from a purely meteorological and climatological perspective. The philosophy behind this method is that the more unusual (with respect to the local climate) a cyclone, cold outbreak, heat wave, or flood of a given intensity is, the higher ranked it must be. The highest ranked events are those that represent the greatest departures from climatology for that locale and time of year. This method not only minimizes the biases discussed earlier, but also accounts for the typical synoptic-scale variability throughout the year. Therefore, a 970-hPa April cyclone will be higher ranked than a 970-hPa January cyclone in the same location.

The second goal of this paper is to examine the temporal distribution of these objectively ranked events. When are these extreme anomalies typically found and how does their distribution change throughout the year, from year to year, or from decade to decade? One question that can be objectively addressed is whether the 1950s and 1960s were a more active time meteorologically, as conventional wisdom often suggests. Further, the relationships between occurrence of these anomalous events and climate indices, such as the North Atlantic oscillation (NAO), the Pacific–North American index (PNA), and El Niño–Southern Oscillation (ENSO), will be examined. Finally, an analysis of expected return periods for extreme events will be presented to give a temporal mindset for anomalies of various intensities.

A detailed description of the methodology is given in section 2, followed by the results of the analysis in section 3. A discussion of the application of these historical lists to forecasted future events is given in section 4 with a concluding summary given in section 5.

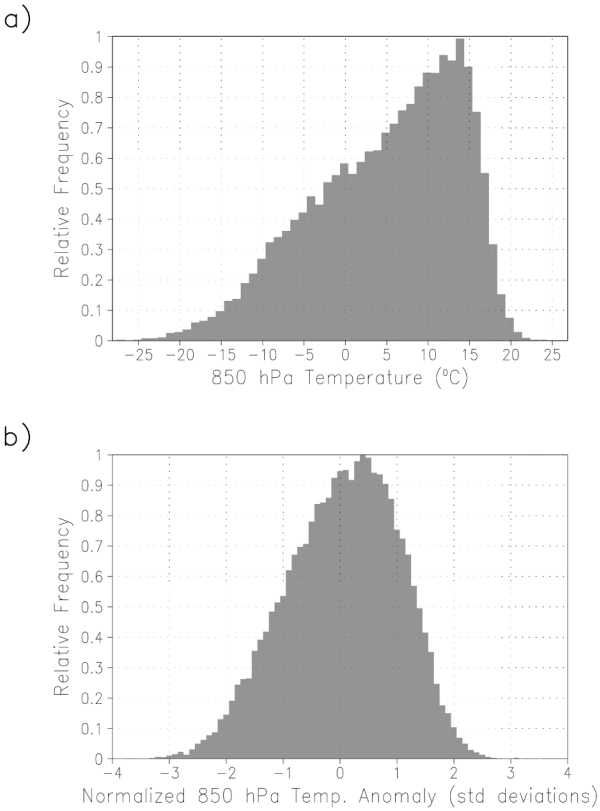

FIG. 1. Relative distribution of (a) 850-hPa temperature and (b) corresponding 850-hPa normalized temperature anomaly for the period 1948–2000 at 40°N, 75°W.

2. Methodology

In order to derive departures from climatology for a specific event, a detailed and comprehensive climatology was developed. An overview of the datasets and definitions used in this approach are described below.

a. Datasets

The National Centers for Environmental Protection (NCEP) reanalysis dataset (Kalnay et al. 1996) was used for this analysis. The global dataset has a 2.5° × 2.5° resolution at 17 pressure levels, extends from 1948 through December 2000, and is updated monthly. For this analysis, four basic meteorological variables from that dataset were used over the range of 1000 hPa through 300 or 200 hPa (Table 1) at 12-h intervals. The climatology (for each 2.5° × 2.5° grid point) was based upon the 1961–90 subset. The analysis of ranking climatological departures was performed for the entire reanalysis period, 1 January 1948 through 31 December 2000. Thus, the rankings provided in this paper represent the analysis of a 53-yr period, of which 23 years (1948–60 and 1991–2000) are therefore an independent sample from the climatological period (1961–90).

Although the data analysis and assimilation method

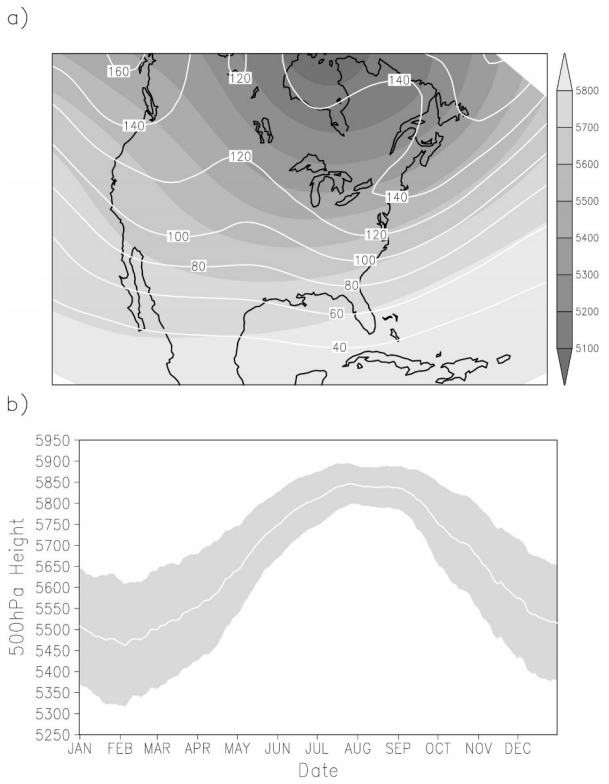

FIG. 2. Example output from the calculated climatology. (a) Mean 500-hPa height (shaded) and standard deviation (contoured) for 1 Jan. (b) Annual distribution of 500-hPa height (white line) and one standard deviation range (shading) for 40°N, 75°W.

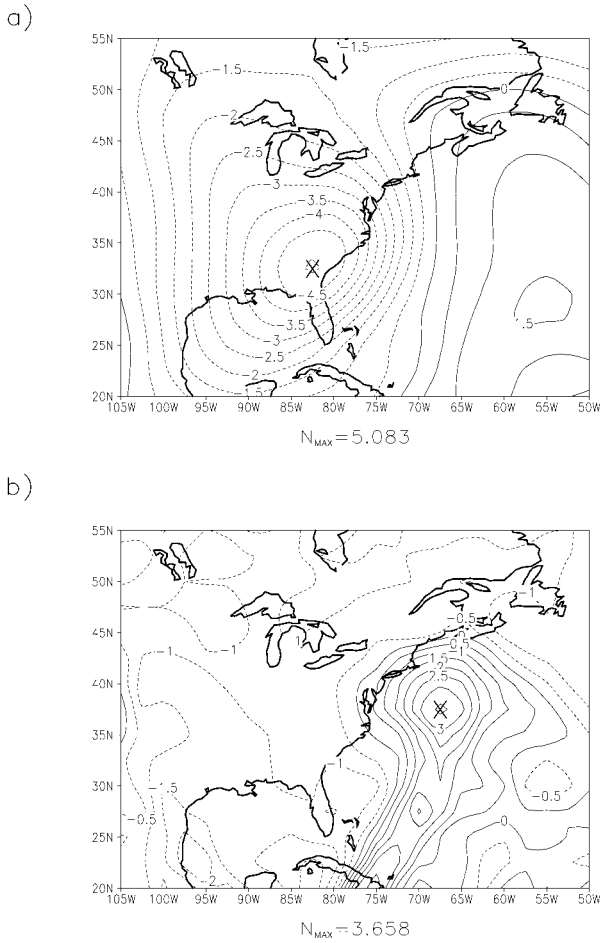

FIG. 3. Example NCEP–NCAR reanalysis-based anomaly fields for 0000 UTC 14 Mar 1993. (a) The 500-hPa height anomaly field and corresponding maximum absolute anomaly are marked by ×. (b) Same as in (a) except for 850-hPa specific humidity anomaly.

used in the NCEP reanalysis project (Kalnay et al. 1996) is a temporally consistent one, there still exist unavoidable yet important changes in the dataset over the 53-yr period. Routine offshore surface observations including buoys became available only in the late 1970s. In addition, the inclusion of satellite-derived products in the data assimilation process was possible only in the last decade. As a consequence of these changes, offshore events may be less accurately represented during the 1950s and 1960s than in the latter decades. These changes in the dataset should be kept in mind when interpreting the results.

Labeling specific events with their impact and informal titles (e.g., ''superstorm'' of 1993) was done using *Storm Data*, *Weatherwise*, and journals when case studies were available. This correlation was performed simply to give the reader a reference for the date, type, and location of the event, not necessarily to directly connect the anomalies with the societal impact. Such conclusions can only be made after detailed case studies and case comparisons that are beyond the scope of this paper. The analysis of events was limited to 25°–50°N and 95°–65°W, to focus on events impacting the eastern half of the United States.

b. Definitions

The normalized departure from climatology (and hence, a measure of event rarity) is given by

$$N = (X - \mu)/\sigma, \tag{1}$$

where X is the value of a variable (e.g., 500-hPa height, 850-hPa temperature, from Table 1), μ is the *daily* mean value for that grid point, and σ is the standard deviation from this daily mean. This process converts a pseudo-normal distribution (e.g., 850-hPa temperature in Fig. 1a) into a standard normal distribution (normalized 850-hPa temperature departure in Fig. 1b). The mean of the distribution shown in Fig. 1b is indeed zero, as dictated by the normalization process shown in (1). However, since the original distribution (Fig. 1a) is skewed, the peak frequency in Fig. 1b is not aligned with zero.

A 21-day running mean was used in the calculation of the daily mean. This was performed instead of a *monthly mean* climatology, the latter of which produces

TABLE 2. Top 20 total normalized departures from climatology (M_{TOTAL}) for the period 1 Jan 1948–31 Dec 2000.

Rank	Date	M_{TOTAL}	Event type and description	Event references
1	0000 UTC 9 Jan 1956	4.950	The Great Atlantic Low	Ludlum (1956)
2	1200 UTC 15 Jan 1995	4.723	Deep Gulf of Mexico storm	
3	0000 UTC 14 Mar 1993	4.577	Superstorm of 1993	Kocin et al. (1995); Dickinson et al. (1997)
4	1200 UTC 11 Jan 1975	4.567	Severe Minnesota Blizzard	
5	1200 UTC 8 Jan 1998	4.536	NE U.S./SE Canada icestorm	J. Gyakum and P. Sisson (1999, personal communication); DeGaetano (2000)
6	1200 UTC 28 Dec 1980	4.470	Deep Carolina coastal low	
7	1200 UTC 17 Mar 1983	4.464	Low-latitude intense cyclone	Dickinson et al. (1997)
8	0000 UTC 26 Nov 1953	4.396	Deep E U.S. storm	
9	0000 UTC 16 Oct 1954	4.392	Extratropical storm Hazel	Knox (1955); Palmén (1958)
10	1200 UTC 8 Jan 1958	4.356	Intense coastal storm	Ludlum (1958a)
11	1200 UTC 19 Jan 1977	4.341	Historic Florida freeze	Schwartz (1977)
12	1200 UTC 19 Jan 1996	4.308	NE U.S. flooding/snowmelt	Leathers et al. (1998)
13	0000 UTC 10 Jan 1978	4.261	Deep NE U.S. storm	
14	1200 UTC 31 Oct 1993	4.232	E U.S. elevation blizzard	Grumm and Nicosia (1997)
15	0000 UTC 4 Feb 1970	4.202	Eastern U.S. storm	
16	1200 UTC 22 Dec 1972	4.199	Deep Gulf of Mexico storm	
17	1200 UTC 11 Dec 1950	4.192	Intense offshore coastal storm	
18	1200 UTC 26 Jan 1978	4.179	The Cleveland superbomb	Gaza and Bosart (1990); Hakim et al. (1995), (1996)
19	0000 UTC 20 Oct 1989	4.179	SE U.S. record cold and snow	
20	1200 UTC 22 Jan 1959	4.176	Severe E U.S. snow/icestorm	Treidl (1959)

ranking artifacts at monthly boundaries. An example climatology field is shown in Fig. 2a, the mean 1 January 500-hPa height field and associated standard deviation. Also, a time series of the mean and standard deviation 500-hPa height for near Philadelphia, Pennsylvania (grid point 40°N, 75°W), is shown to illustrate the relatively smooth climatology that results when a 21-day running mean is used (Fig. 2).

According to (1), a value of $N = -3$ means the field is three standard deviations below average for that location and day (a significant, but not extreme, departure). An example anomaly field is provided in Fig. 3. 500-hPa normalized height anomaly fields (Fig. 3a) and 850-hPa normalized moisture anomaly (Fig. 3b) for 0000 UTC 14 March 1993, the infamous superstorm of 1993 (SS93). The ×s indicate the maximum value of N (N_{MAX}) for the given field over the domain specified earlier. Each event in the 53-yr period has four anomaly measures: one each for height, temperature, wind, and moisture. Each of these four measures is the mass-weighted mean anomaly, using the pressure levels available in the reanalysis dataset (Table 1):

$$M_{\text{HEIGHT}} = \frac{1}{n} \sum_{p=1000\,\text{hPa}}^{p=200\,\text{hPa}} |N^{Z}_{\text{MAX}}(p)| \tag{2}$$

$$M_{\text{TEMP}} = \frac{1}{n} \sum_{p=1000\,\text{hPa}}^{p=200\,\text{hPa}} |N^{T}_{\text{MAX}}(p)| \tag{3}$$

$$M_{\text{WIND}} = \frac{1}{n} \sum_{p=1000\,\text{hPa}}^{p=200\,\text{hPa}} |N^{UV}_{\text{MAX}}(p)| \tag{4}$$

$$M_{\text{MOIST}} = \frac{1}{n} \sum_{p=1000\,\text{hPa}}^{p=300\,\text{hPa}} |N^{Q}_{\text{MAX}}(p)|. \tag{5}$$

For each of the summations above, an interpolating pressure increment of 25 hPa was used to more accurately calculate the mass-weighted mean. The total tropospheric anomaly (M_{TOTAL}) is then the average of the four components above:

$$M_{\text{TOTAL}} = (M_{\text{HEIGHT}} + M_{\text{TEMP}} + M_{\text{WIND}} + M_{\text{MOIST}})/4. \tag{6}$$

Thus, the most extreme events will be those that have large departures from climatology extending the full depth of the troposphere for each of the four basic variables. For the wind anomaly, the maximum anomaly of either component (u or v) was used. Typically the v component produced the larger anomalies.

When calculating (2)–(5), the individual anomalies were allowed to be displaced from one another, up to the full distance of the analyzed domain (25°–50°N, 95°–65°W). A height anomaly may be maximized at lower latitudes, while the associated moisture anomaly may be maximized at higher latitudes. Further, the maximum height anomaly at 850 hPa is likely to be downstream from the maximum height anomaly at 500 hPa (e.g., Fig. 3). This diagnosis freedom also allows for the full tilt (both horizontal and vertical) of events to be accounted for when the total anomaly magnitude [M_{TOTAL}, (6)] is determined. Further, it is an important caveat to note that we define the M_{TOTAL} value to refer to the vertically integrated maximum anomaly across the domain. Therefore, only one M_{TOTAL} value is defined at each 12-h time period.

Tropical cyclones within the domain were excluded (the entire domain) for two reasons: 1) they are of smaller scale than the events this analysis is intended to include, and 2) since the projected data is 2.5° resolution, the grids grossly underestimate the true magnitude of the tropical cyclone normalized anomaly. Since the true

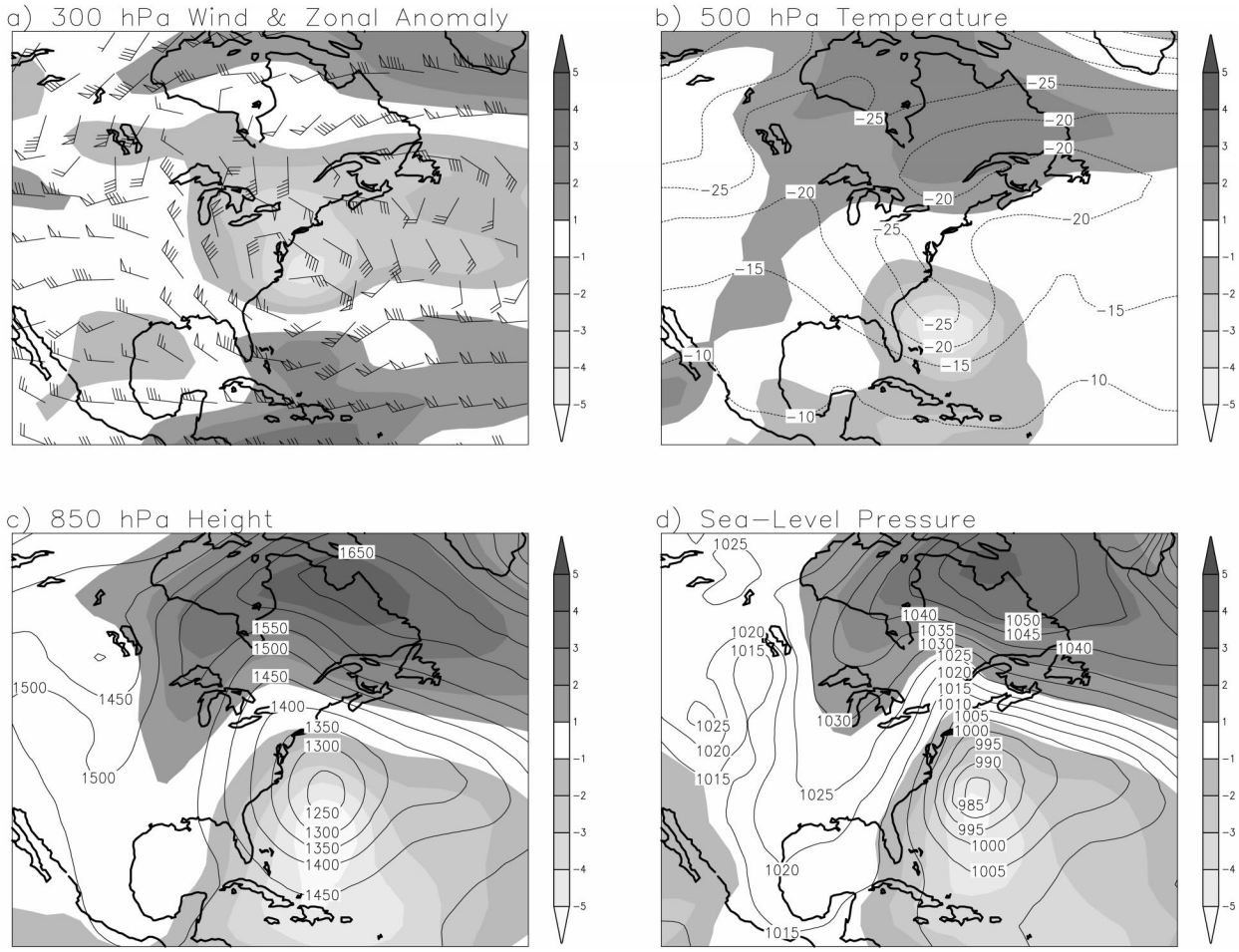

FIG. 4. Conventional analyses (contoured) and corresponding anomaly fields (shaded) for the top-ranked event since 1948—The Great Atlantic Low of 0000 UTC 9 Jan 1956. (a) 300-hPa wind and zonal anomaly, (b) 850-hPa temperature and anomaly, (c) 850-hPa height and anomaly, and (d) mean sea level pressure and anomaly.

anomaly magnitude was greatly underestimated, it was believed to be misleading to include the tropical cyclone statistics as part of the ranking. If the true tropical cyclone intensity was resolved, the top 10 events of each month from June through September would be tropical cyclones. However, because of the 2.5° × 2.5° resolution, only a fraction would actually make the rankings, even though they are truly the largest summertime anomalies. An exception to this rule was made for tropical cyclones that have undergone extratropical transition. In cases where a tropical cyclone had undergone extratropical transition according to the National Hurricane Center historical ''best track'' dataset (Jarvinen et al. 1984), the cyclone was allowed to remain in the database if the analyzed cyclone intensity was well represented by the reanalysis fields. Only five such cases appear in the rankings to follow: Hazel (1954), Agnes (1972), Hugo (1989), the ''unnamed'' hurricane of 1991 [or ''perfect storm'' of Junger (1997)], and Opal (1995).

For each 12-h period from 1 January 1948 through 31 December 2000, an M_{TOTAL} value was calculated using the method just described. After the tropical cyclone periods were removed, these anomalies were then sorted. For each ranked event, only the highest-ranked time and date was used. Thus, an event could not contribute toward more than one place in the rankings, even if it ranked for more than 12 h.

3. Results

The results are divided into two sections: rankings and temporal distribution. As discussed in the methodology, the results shown here are valid only for the southeastern half of North America, from 25° to 50°N and from 65° to 95°W.

a. Rankings

The top 20 total anomalies (M_{TOTAL}) of the 53-yr period are summarized first, followed by a presentation of the top 10 anomalies for each of the four component

variables (M_{HEIGHT}, M_{TEMP}, M_{WIND}, and M_{MOIST}) and the top 10 anomalies for each month.

1) TOP 20 LARGEST NORMALIZED ANOMALIES FROM 1 JANUARY 1948 TO 31 DECEMBER 2000

The top 20 largest climatological anomalies (Table 2; information from *Storm Data*, NOAA 1959–2000) represent the most spectacular climate departures of the past half-century. The magnitudes of these top 20 anomalies range from $M_{TOTAL} = 4.176$ to $M_{TOTAL} = 4.950$. Of particular note within the events listed in Table 2 are SS93 [ranked third; Kocin et al. (1995); Dickinson et al. (1997)], the historic southern Florida freeze and Miami snow of 1977 [ranked 11th; Schwartz (1977)], the historic New England and Quebec icestorm of 1998 [ranked 5th; J. Gyakum and P. Sisson (1999, personal communication) DeGaetano (2000)], extratropical hurricane Hazel from 1954 [ranked 9th; Knox (1955); Palmén (1958)], the great Northeast snowmelt and flood of 1996 [ranked 12th; Leathers et al. (1998)], and the Cleveland ''superbomb'' of 1978 [ranked 18th; Gaza and Bosart (1990); Hakim et al. (1995, 1996)].

Note that nearly one-third of the events shown in the top 20 are not historically known for having a major impact upon the population or economy of the United States (Table 2: ranks 2, 6, 8, 15, 16, and 17). Documentation of these events could not be found with the literature nor could reports of significant damage or impact be found within *Storm Data*. (Although synoptic analyses for each of the top 20 events are beyond the scope of this paper, they are available online at: http://eyewall.met.psu.edu/.)

The most anomalous synoptic-scale event for the eastern United States of the past 53 years stands alone as a record. The event was referred to by D. Ludlum (1956) as ''The Great Atlantic Low.'' The associated M_{TOTAL} was 4.950, at least 0.2 standard deviations higher than the second-ranked event, a leap larger than any other two consecutive events in the top 20. Given this disparity between first and second place, this event may well hold the top position for another half-century. The surface and upper-air anomaly fields for 0000 UTC 9 January 1956 are shown in Fig. 4, since synoptic-scale fields are not available as part of Ludlum's summary. Further, since the top-ranked event is located offshore and otherwise obscure, we quote below a paragraph from Ludlum's (1956) summary to accompany the anomaly fields shown in Fig. 4:

> The Great Atlantic Low—The index of westerly flow reached its all-time low for this period of the year, and for any period, on 7–11 January 1956. Just off the Middle Atlantic coast a deep, almost stationary, low was found with a central pressure on the 9th below 29.00 inches. Directly to the north over extreme northern Quebec an anticyclone of great magnitude was located with a central pressure reported above 31.40 inches, the highest pressure ever noted in that region. Zones of different precipitation were oriented longitudinally rather than along lines of latitude. For the week ending 15 January, northern Maine's temperature averaged 24 degrees above normal, while points in central Florida had readings 15 degrees below normal. From 8 to 14 January the mercury did not dip below freezing at Caribou, while Florida had nighttime readings below freezing most every night during this period. The Great Atlantic Low of early January 1956 appears to have been without a parallel in recorded weather history. No such occurrence appears in the series of historical weather maps which commence in 1899.

This top-ranked event is made more impressive since it occurs in a data-sparse region, where the reanalyses may be underestimating the true intensity.

2) TOP 10 ANOMALIES BY VARIABLE

As explained in the methodology, every event during the 53-yr period has four anomaly magnitudes associated with it: one each for height, temperature, wind, and moisture Eqs. (2)–(5). In Tables 3a–d, the top 10 anomalies for each of these four variables are listed.

The largest value of M_{HEIGHT} (6.847, Table 3a) was associated with a deep Gulf of Mexico cyclone in 1983. Prior to SS93, this 1983 cyclone set the record for the lowest non–tropical cyclone sea level pressure ever measured over the Gulf of Mexico (Dickinson et al. 1997). Most of the remaining top 10 height anomalies are associated with deep wintertime East Coast troughs or closed cyclones at lower latitudes (e.g., SS93). Of particular exception is the post-Agnes extratropical cyclone in June 1972 (DiMego and Bosart 1982a,b; Bosart and Dean 1991).

The largest value of M_{TEMP} (5.355, Table 3b) was associated with a remarkable early season record cold outbreak in October 1989 that produced early season snow well into the southeast United States (NOAA 1959–2000, vol. 31). The second largest value of M_{TEMP} (5.020, Table 3b) was associated with the Florida freeze and Miami snow of January 1977 (Schwartz 1977). This event produced the only snowflakes ever recorded on Miami Beach and in the Bahamas (NOAA 1959–2000, vol. 19; Schwartz 1977). The other top-ranked M_{TEMP} events are predominantly associated with early or late season snowstorms.

The largest M_{WIND} values (Table 3c) are associated with intense cyclones at lower latitudes. The largest wind anomaly in the 53-yr period (M_{WIND} of 5.515) was associated with a deep Gulf of Mexico storm in April 1997. The storm produced an 80-kt jet at 500 hPa over the Gulf of Mexico, which intensified to a 150-kt jet at 200 hPa over Virginia. Such values would have been impressive in January; that they occurred in late April is what propels this event to the top of Table 3c. The second-ranked M_{WIND} value (5.073) was associated with SS93. The third-ranked M_{WIND} value (5.012) was as-

TABLE 3a. Top 10 normalized height departures from climatology.

Rank	Date	M_{HEIGHT}	Event type/description	Event references
1	1200 UTC 17 Mar 1983	6.847	Low-latitude intense cyclone	Dickinson et al. (1997)
2	0000 UTC 9 Jan 1956	6.120	The Great Atlantic Low	Ludlum (1956)
3	1200 UTC 19 Jan 1977	5.698	Historical Florida freeze	Schwartz (1977)
4	1200 UTC 11 Dec 1967	5.419	Deep Gulf of Mexico storm	
5	0000 UTC 28 May 1973	5.404		
6	0000 UTC 21 Nov 1952	5.358	Record Appalachian snowstorm	Ludlum (1952)
7	1200 UTC 23 Jun 1972	5.286	Extratropical storm Agnes	DiMego and Bosart (1982a,b); Bosart and Dean (1991)
8	0000 UTC 3 Feb 1998	5.252		
9	1200 UTC 13 Mar 1993	5.195	Superstorm of 1993	Kocin et al. (1995); Dickinson et al. (1997)
10	1200 UTC 8 Jan 1958	5.193	Intense coastal storm	Ludlum (1958a)

TABLE 3b. Top 10 normalized temperature departures from climatology.

Rank	Date	M_{TEMP}	Event type and description	Event references
1	0000 UTC 20 Oct 1989	5.355	SE U.S. record cold and snow	
2	1200 UTC 19 Jan 1977	5.020	Historical Florida freeze	Schwartz (1977)
3	1200 UTC 26 Nov 1953	4.959		
4	1200 UTC 7 May 1992	4.880		
5	1200 UTC 2 Nov 1966	4.835	Heavy central Appalachian snowstorm	
6	0000 UTC 2 Dec 1999	4.830		
7	0000 UTC 10 Sep 1998	4.816		
8	1200 UTC 18 Sep 1981	4.716		
9	1200 UTC 4 Aug 1956	4.683		
10	1200 UTC 28 Apr 1992	4.620		

TABLE 3c. Top 10 normalized wind departures from climatology.

Rank	Date	M_{WIND}	Event type and description	Event references
1	1200 UTC 28 Apr 1997	5.515	Strong late season Gulf storm	
2	0000 UTC 14 Mar 1993	5.073	Superstorm of 1993	Kocin et al. (1995); Dickinson et al. (1997)
3	0000 UTC 26 Nov 1950	5.013	Historic E. U.S. storm	Bristor (1951)
4	1200 UTC 9 Jan 1956	4.883	The Great Atlantic Low	Ludlum (1956)
5	0000 UTC 27 Jun 1974	4.759	Transitioned subtropical storm	
6	1200 UTC 28 Dec 1980	4.742	Deep Carolina coastal low	
7	1200 UTC 16 Jun 1989	4.714	Widespread SE/mid-Atlantic severe outbreak	
8	0000 UTC 12 Mar 1996	4.675	Deep offshore coastal storm	
9	0000 UTC 12 Feb 1981	4.672	Extreme amplitude E. U.S. trough	
10	1200 UTC 1 Aug 1972	4.584		

TABLE 3d. Top 10 normalized moisture departures from climatology.

Rank	Date	M_{MOIST}	Event type and description	Event references
1	1200 UTC 15 Jan 1995	7.734	Deep Gulf of Mexico storm	
2	1200 UTC 22 Jan 1959	7.359	Severe E. U.S. snow-/icestorm	Treidl (1959)
3	1200 UTC 8 Jan 1998	7.104	NE U.S./SE Canada icestorm	J. Gyakum and P. Sisson (1999, personal communication); DeGaetano (2000)
4	0000 UTC 20 Jan 1996	6.948	NE U.S. flooding/snowmelt	Leathers et al. (1998)
5	1200 UTC 11 Jan 1975	6.767	Severe Minnesota blizzard	
6	1200 UTC 4 Jan 1950	6.654		
7	0000 UTC 10 Jan 1978	6.536		
8	1200 UTC 26 Jan 1950	6.461		
9	0000 UTC 24 Jan 1999	6.454		
10	0000 UTC 5 Jan 1997	6.285		

TABLE 4a. Top 10 Jan total normalized departures from climatology.

Rank	Date	M_{TOTAL}	Event type and description	Event references
1	0000 UTC 9 Jan 1956	4.950	The Great Atlantic Low	Ludlum (1956)
2	1200 UTC 15 Jan 1995	4.722	Deep Gulf of Mexico storm	
3	1200 UTC 11 Jan 1975	4.566	Severe Minnesota blizzard	
4	1200 UTC 8 Jan 1998	4.536	NE U.S./SE Canada icestorm	J. Gyakum and P. Sisson (1999, personal communication); DeGaetano (2000)
5	1200 UTC 8 Jan 1958	4.356		
6	1200 UTC 19 Jan 1977	4.340	Historic Florida freeze	Schwartz (1977)
7	1200 UTC 19 Jan 1996	4.307	NE U.S. flooding/snowmelt	Leathers et al. (1998)
8	0000 UTC 10 Jan 1978	4.260	Deep NE U.S. storm	
9	1200 UTC 26 Jan 1978	4.179	Cleveland superbomb	Gaza and Bosart (1990); Hakim et al. (1995, 1996)
10	1200 UTC 22 Jan 1959	4.176	Severe E. U.S. snow-/icestorm	Treidl (1959)

TABLE 4b. Top 10 Feb total normalized departures from climatology.

Rank	Date	M_{TOTAL}	Event type and description
1	0000 UTC 4 Feb 1970	4.201	
2	0000 UTC 12 Feb 1981	4.041	Extreme amplitude E. U.S. trough
3	0000 UTC 12 Feb 1999	3.892	
4	1200 UTC 3 Feb 1998	3.863	
5	0000 UTC 23 Feb 1981	3.788	
6	1200 UTC 10 Feb 1966	3.728	
7	1200 UTC 13 Feb 1962	3.710	
8	1200 UTC 21 Feb 1953	3.701	
9	0000 UTC 21 Feb 1955	3.598	
10	0000 UTC 24 Feb 1989	3.571	

TABLE 4c. Top 10 Mar total normalized departures from climatology.

Rank	Date	M_{TOTAL}	Event type and description	Event references
1	0000 UTC 14 Mar 1993	4.576	Superstorm of 1993	Kocin et al. (1995); Dickinson et al. (1997)
2	1200 UTC 17 Mar 1983	4.464	Low-latitude intense cyclone	Dickinson et al. (1997)
3	1200 UTC 11 Mar 1996	3.931		
4	0000 UTC 16 Mar 1990	3.856	NE U.S. heat/SE U.S. flooding	
5	1200 UTC 21 Mar 1958	3.789	Heavy NE elevation snowstorm	Ludlum (1958b)
6	0000 UTC 7 Mar 1987	3.781	North-central/NE U.S. heat wave	
7	1200 UTC 4 Mar 1991	3.725		
8	0000 UTC 18 Mar 1973	3.634		
9	1200 UTC 5 Mar 1964	3.617		
10	1200 UTC 23 Mar 1968	3.593		

TABLE 4d. Top 10 Apr total normalized departures from climatology.

Rank	Date	M_{TOTAL}	Event type and description
1	1200 UTC 28 Apr 1997	4.133	
2	0000 UTC 1 Apr 1987	3.911	SE U.S. record cold outbreak
3	0000 UTC 30 Apr 1953	3.904	
4	1200 UTC 14 Apr 1980	3.766	
5	0000 UTC 29 Apr 1992	3.731	
6	1200 UTC 5 Apr 1977	3.723	
7	0000 UTC 17 Apr 1984	3.721	
8	0000 UTC 12 Apr 1988	3.706	S Appalachian snowstorm
9	1200 UTC 18 Apr 1983	3.680	
10	1200 UTC 30 Apr 1996	3.580	

sociated with a damaging November 1950 snow- and windstorm that produced surface winds in excess of 100 mph from New York City through New England (Bristor 1951).

Many rare storms (bottom half of Table 2) do not have top-ranked moisture anomalies (Table 3d) because they are deep cutoff cyclones at lower latitudes (where climatological mean moisture values are highest) with-

out a significant positive moisture anomaly. The largest moisture anomaly values occur at high latitudes (greater than 40°N) in the winter when climatological mean values are lowest but variability is large. Examination of the top 10 moisture anomalies (M_{MOIST}, Table 3d) of the past 53 years reveals many very familiar events. Fourth ranked is the infamous Northeast (post-1996 blizzard) snowmelt and flooding of January 1996 (Leathers et al. 1998). Another recent event of interest (ranked third) is the major Northeast and Canada icestorm of 1998 where many went without electricity for weeks, including 10% of the Canadian population (J. Gyakum and P. Sisson 1999, personal communication; DeGaetano 2000). The severe Minnesota blizzard of 1975, often called the northern plains' ''storm of the century,'' shows up in the list as the fifth-highest M_{MOIST} value.

Nearly half of the events listed in Tables 3a–d do not make the top 20 total anomalies (Table 2). This suggests that it is exceptionally rare for a pattern to develop where each of the four variables simultaneously achieves extreme levels. For example, in many cases where M_{TEMP} and M_{HEIGHT} are large (e.g., as a result of a deep trough), values of absolute moisture are usually less (since the atmosphere is colder than average and fast flow precludes development of large, sustained moisture anomalies) and thus M_{MOIST} is smaller. This limiting relationship between M_{TEMP} and M_{MOIST} is further dictated by the nonlinear relationship between saturation vapor pressure and temperature.

3) TOP 10 ANOMALIES BY MONTH

When the rankings are expanded to the top events by month (Tables 4a–l), a great many additional well-known events appear. Such monthly analysis gives a more detailed perspective on what types of record events (and of what magnitude) occur during each month, and how they vary from month to month. This monthly breakdown is also significant because there is a clear monthly bias in Table 2, with most spring and summer months greatly underrepresented.

Top monthly ranked significant winter events include two intense coastal storms of late December 1997 (Table 4l). Impressively, all 10 top January events (Table 4a) are found in Table 2. Conversely, however, there are surprisingly few memorable events in the top 10 February anomalies, a result that has no clear meteorological explanation. Top-ranked springtime events are predominantly record-setting cold or heat waves, or the occasional late season intense cyclone. As mentioned, while not included here, the largest summertime anomalies are major tropical cyclones. However, for those summer events included here, top ranked are the major flood and severe weather outbreak of 1996 (Pearce 1997) and the massive flooding caused by an extratropical Hurricane Agnes (DiMego and Bosart 1982a,b; Bosart and Dean 1991).

The autumn top-ranked anomalies are the most varied in type. Top ranked in October is extratropical storm Hazel (Knox 1955; Palmén 1958) and a particularly devastating 1993 early season snowfall along the elevated areas of the Appalachians (Grumm and Nicosia 1997). Also ranked in October is the Halloween storm of 1991, also known as the ''perfect storm'' (Cardone et al. 1996; Junger 1997), and extratropical storm Opal (1995). In November, two additional cases of interest are ranked: the aforementioned early season snowstorm

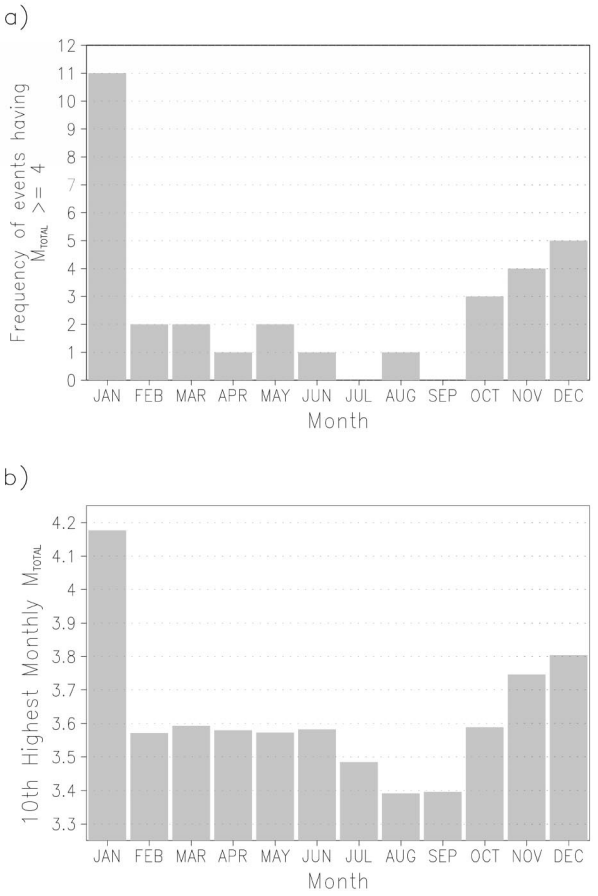

FIG. 5. (a) Monthly frequency of events having an M_{TOTAL} of 4 or greater, as noted in Table 4. (b) Distribution of the 10th highest M_{TOTAL} value by month.

TABLE 4e. Top 10 May total normalized departures from climatology.

Rank	Date	M_{TOTAL}
1	0000 UTC 28 May 1973	4.131
2	1200 UTC 15 May 1976	4.076
3	1200 UTC 7 May 1992	3.864
4	0000 UTC 7 May 1982	3.781
5	0000 UTC 26 May 1979	3.718
6	0000 UTC 13 May 1960	3.656
7	0000 UTC 6 May 1950	3.636
8	1200 UTC 20 May 1994	3.632
9	1200 UTC 17 May 1984	3.585
10	1200 UTC 29 May 1953	3.573

TABLE 4f. Top 10 Jun total normalized departures from climatology.

Rank	Date	M_{TOTAL}	Event type and description	Event references
1	0000 UTC 13 Jun 1990	4.030		
2	1200 UTC 29 Jun 1981	3.996		
3	1200 UTC 27 Jun 1974	3.984	Transitioned subtropical storm	
4	1200 UTC 23 Jun 1972	3.974	Extratropical storm Agnes	DiMego and Bosart (1982a,b); Bosart and Dean (1991)
5	0000 UTC 4 Jun 1955	3.957		
6	1200 UTC 11 Jun 1955	3.914		
7	0000 UTC 27 Jun 1985	3.775		
8	1200 UTC 28 Jun 1957	3.664		
9	1200 UTC 2 Jun 1984	3.641		
10	1200 UTC 10 Jun 1977	3.582		

TABLE 4g. Top 10 Jul total normalized departures from climatology.

Rank	Date	M_{TOTAL}	Event type and description	Event references
1	1200 UTC 14 Jul 1990	3.906		
2	1200 UTC 13 Jul 1975	3.653		
3	0000 UTC 2 Jul 1988	3.622	NE U.S. record Jul cold	
4	1200 UTC 28 Jul 1994	3.567		
5	0000 UTC 12 Jul 1979	3.558		
6	1200 UTC 20 Jul 1996	3.535	NE U.S. severe outbreak	Pearce (1997)
7	1200 UTC 15 Jul 1967	3.534		
8	1200 UTC 10 Jul 1963	3.525		
9	0000 UTC 6 Jul 1993	3.499		
10	0000 UTC 11 Jul 1983	3.485		

TABLE 4h. Top 10 Aug total normalized departures from climatology.

Rank	Date	M_{TOTAL}	Event type and description
1	1200 UTC 22 Aug 1973	4.077	Deep Gulf of Mexico storm
2	1200 UTC 3 Aug 1964	3.811	
3	1200 UTC 7 Aug 1950	3.735	
4	1200 UTC 17 Aug 1980	3.722	
5	1200 UTC 13 Aug 2000	3.589	Deep cutoff and mid-Atlantic flood
6	1200 UTC 26 Aug 1951	3.528	
7	1200 UTC 21 Aug 1961	3.505	
8	1200 UTC 3 Aug 1989	3.497	
9	1200 UTC 4 Aug 1956	3.496	
10	1200 UTC 11 Aug 1954	3.391	

TABLE 4i. Top 10 Sep total normalized departures from climatology.

Rank	Date	M_{TOTAL}	Event type and description	Event references
1	1200 UTC 19 Sep 1981	3.793		
2	1200 UTC 23 Sep 1989	3.598	Extratropical storm Hugo and early snow	Abraham et al. (1991)
3	0000 UTC 5 Sep 1997	3.588		
4	1200 UTC 26 Sep 1982	3.562		
5	0000 UTC 4 Sep 1998	3.546		
6	0000 UTC 24 Sep 1994	3.516		
7	1200 UTC 24 Sep 1975	3.514		
8	1200 UTC 6 Sep 1988	3.436	3-day record cold wave	
9	1200 UTC 22 Sep 1983	3.423		
10	1200 UTC 13 Sep 1951	3.396		

in 1966 and a record cold outbreak of 1989. This record cold outbreak followed a massive severe thunderstorm outbreak and derecho in the northeast United States (NOAA 1989; Ruscher and Condo 1996a,b).

b. Temporal variability

In the public mindset, the severity of a winter season is usually most greatly related to amount of snowfall,

TABLE 4j. Top 10 Oct total normalized departures from climatology.

Rank	Date	M_{TOTAL}	Event type and description	Event references
1	0000 UTC 16 Oct 1954	4.391	Extratropical storm Hazel	Knox (1955); Palmén (1958)
2	1200 UTC 31 Oct 1993	4.232	E U.S. elevation blizzard	Grumm and Nicosia (1997)
3	0000 UTC 20 Oct 1989	4.179	SE U.S. record cold and snow	
4	1200 UTC 25 Oct 1959	3.915		
5	1200 UTC 30 Oct 1991	3.856	The ''perfect storm''	Cardone et al. (1996); Junger (1997)
6	0000 UTC 6 Oct 1995	3.782	Extratropical storm Opal	
7	1200 UTC 13 Oct 1997	3.699		
8	1200 UTC 9 Oct 1952	3.631		
9	0000 UTC 15 Oct 1955	3.598		
10	1200 UTC 17 Oct 1994	3.589		

TABLE 4k. Top 10 Nov total normalized departures from climatology.

Rank	Date	M_{TOTAL}	Event type and description	Event references
1	0000 UTC 26 Nov 1953	4.396		
2	1200 UTC 2 Nov 1966	4.145	Heavy central Appalachian snowstorm	
3	0000 UTC 21 Nov 1952	4.081	Record appalachian snowstorm	Ludlum (1952)
4	0000 UTC 17 Nov 1989	4.005	NE cold after severe outbreak	Ruscher and Condo (1996a,b)
5	1200 UTC 12 Nov 1968	3.937	Severe coastal storm	
6	1200 UTC 5 Nov 1950	3.895		
7	0000 UTC 26 Nov 1950	3.850	Historic E U.S. storm	Bristor (1951)
8	1200 UTC 20 Nov 1954	3.790		
9	0000 UTC 4 Nov 1951	3.787	E U.S. autumn snowstorm	Ludlum (1951)
10	1200 UTC 18 Nov 1958	3.746		

TABLE 4l. Top 10 Dec total normalized departures from climatology.

Rank	Date	M_{TOTAL}	Event type and description
1	1200 UTC 28 Dec 1980	4.469	Deep Carolina coastal low
2	1200 UTC 22 Dec 1972	4.199	Deep Gulf of Mexico storm
3	1200 UTC 11 Dec 1950	4.192	
4	0000 UTC 16 Dec 1992	4.101	
5	1200 UTC 14 Dec 1997	4.084	Deep Gulf of Mexico storm
6	1200 UTC 11 Dec 1967	3.985	Deep Gulf of Mexico storm
7	0000 UTC 10 Dec 1957	3.926	
8	0000 UTC 15 Dec 1953	3.923	
9	0000 UTC 30 Dec 1997	3.922	Intense NE coastal storm
10	0000 UTC 11 Dec 1981	3.804	

the length of time that snowfall remained on the ground, the degree of public preparedness, and the paralyzing nature of the storm. While these factors are clearly important societal and economic issues, they do not describe objectively the variability of past extreme events. However, using the historical database of calculated M_{TOTAL} values, we can examine more objectively whether earlier decades were indeed a time of greater frequency of extreme events.

1) ANNUAL CYCLE

This methodology described in section 2 accounts for the typical synoptic-scale variability found throughout the year. Thus, a cyclone of a fixed departure from average will produce a larger normalized anomaly in the summer than it will in the winter. However, the distribution of events leading to the calculation of mean and standard deviation is most greatly dominated by events within one standard deviation of average (Fig. 1b). Rare or extreme events are few in number and do not impact the mean or standard deviation significantly. Therefore, the frequency of occurrence of rare events (anomalies more than 4 standard deviations from average) can be nearly independent of the annual cycle of the standard deviation (Fig. 2b). Consequently, *rare* event frequency and magnitude will still vary throughout the year.

Figure 5a shows the monthly frequency distribution of events having an M_{TOTAL} value of 4 or greater. A clear maximum in frequency exists during the winter with a minimum during the summer. Although major departures from climatology are still possible in the summer, the magnitude of M_{TOTAL} typically cannot reach 4 or greater because the nonlinear processes that lead to such great anomalies (baroclinic cyclogenesis, frontogenesis, advection, and shear) are greatly limited in the summer. Thus, although the atmosphere is more variable in the winter (and this increased variability is accounted for

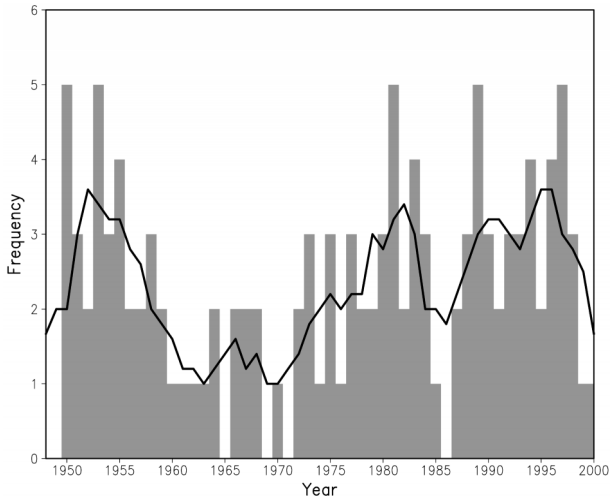

FIG. 6. Interannual frequency of extreme activity for the period 1948–2000. Shaded frequency plotted is the number of monthly top 10 events occurring by year (see Table 4). The solid line is a 5-yr running mean.

in section 2), the winter season will still produce the greatest normalized anomalies. A more resistant statistic illustrating the annual cycle would be the 10th highest monthly M_{TOTAL} value (Fig. 5b). A similar cycle exists, with a maximum of M_{TOTAL} in the winter season and a minimum in the late summer.

2) INTERANNUAL VARIABILITY AND CLIMATE INDICES

In section 3b(1) considerable seasonal variability in the occurrence of rare anomaly events (Fig. 5) was found. We next examine how the occurrence of rare events varies from year to year, and whether specific decades were more prone to experiencing these extreme events (Fig. 6). There are randomly spaced periods of 2–4 yr of alternating above average and below average record events, although no regular short-term cycle of variability is evident. The approximate decadal trend, however, can be seen when a 5-yr running mean (solid line in Fig. 6) is applied to the time series in Fig. 6. The 1950s were a decade of above average frequency of monthly top 10 events, with the 1960s and early 1970s showing a clear decline in the frequency of monthly top 10 events. With the exception of the middle 1980s, the period from 1980 through 1999 was a period of increased activity of rare events. Certainly the period of record here is not sufficiently long to determine definitively a decadal signal. However, there is strong evidence in Fig. 6 that there are long-term patterns to the frequency of rare event frequency. The maximum of rare event frequency in the 1950s (when data density was at a minimum) offers support that this long-term cycle in event frequency is a true atmospheric trend rather than an artificial one solely associated with a change in data density.

Thus far we have focused on the frequency distribution of extreme events. This is a narrow percentage of the total distribution of events (Fig. 1b). Since extreme events are so rare, the impact of climate signals and patterns may be elusive thus far. Further insight may be gained by examining the full 53-yr time series of anomaly magnitude when the annual cycle is removed through a 365-day running mean (Fig. 7). If the only periodicity within Fig. 7 were the annual cycle, then Fig. 7 would exhibit a nearly flat distribution. However, when we remove the annual cycle in this fashion, we find regular interannual and decadal cycles remain (Figs. 7a–e). Figures 7a–d displays the 53-yr time series of each of the four component anomalies: M_{HEIGHT}, M_{TEMP}, M_{WIND}, and M_{MOIST}, respectively. The corresponding M_{TOTAL} value is shown in Fig. 7e. Maxima in activity are found in the middle 1950s, again in the early 1980s, and after 1995 (Fig. 7e). A sustained period of decreased activity is found in the 1960s and 1970s and again in the late 1980s and early 1990s.

The trend in M_{MOIST} (Fig. 7d) has an additional long-term trend that is not seen in the other three components (M_{HEIGHT}, M_{TEMP}, and M_{WIND}). Prior to 1960, M_{MOIST} is large but steadily decreasing, followed by an extended period of below average M_{MOIST} until 1978. After 1978, a period of generally above average M_{MOIST} is observed. While this suggests a long-term periodicity ($>$30–40 yr), clearly the 53-yr analysis period is not long enough to conclusively determine this climate-scale moisture periodicity and its potential sources (e.g., oceanic salinity and temperature cycles).

In addition to the decadal trends found in Figs. 7a–e, there is also strong evidence of interannual trends. In each of the panels, irregularly spaced periods of 2–5 yr are suggested. Based upon previous research into interannual variability in temperature and precipitation patterns across North America and Europe (van Loon and Rogers 1978), a comparison of M_{TOTAL} (Fig. 7e) to the PNA, NAO, and Southern Oscillation index (SOI) indices (Figs. 7F–h) appears warranted. The climate index data were obtained from the NCEP Climate Prediction Center (CPC) (which is available online http://www.cpc.ncep.noaa.gov/data/indices/). The respective correlations between M_{TOTAL} and each climate index are given as the R value in each of the three panels. Expectedly, the NAO has slight correlation (-0.21) with M_{TOTAL}. As the NAO becomes increasingly negative, the polar jet stream over North America becomes increasingly meridional. As this happens, the likelihood for a larger M_{TOTAL} increases, giving the weak negative correlation. The SOI also has a marginal correlation (-0.22), which suggests that as the SOI becomes increasingly negative (stronger El Niño), the activity over the domain (M_{TOTAL}) increases slightly. However, this correlation is again weak (R^2 values are at most 0.05), which suggests that neither NAO or SOI separately explain more than 5% of the observed variability in M_{TOTAL}. Further, when a time-lag correlation (varying between $+6$ and -6 months) was applied to

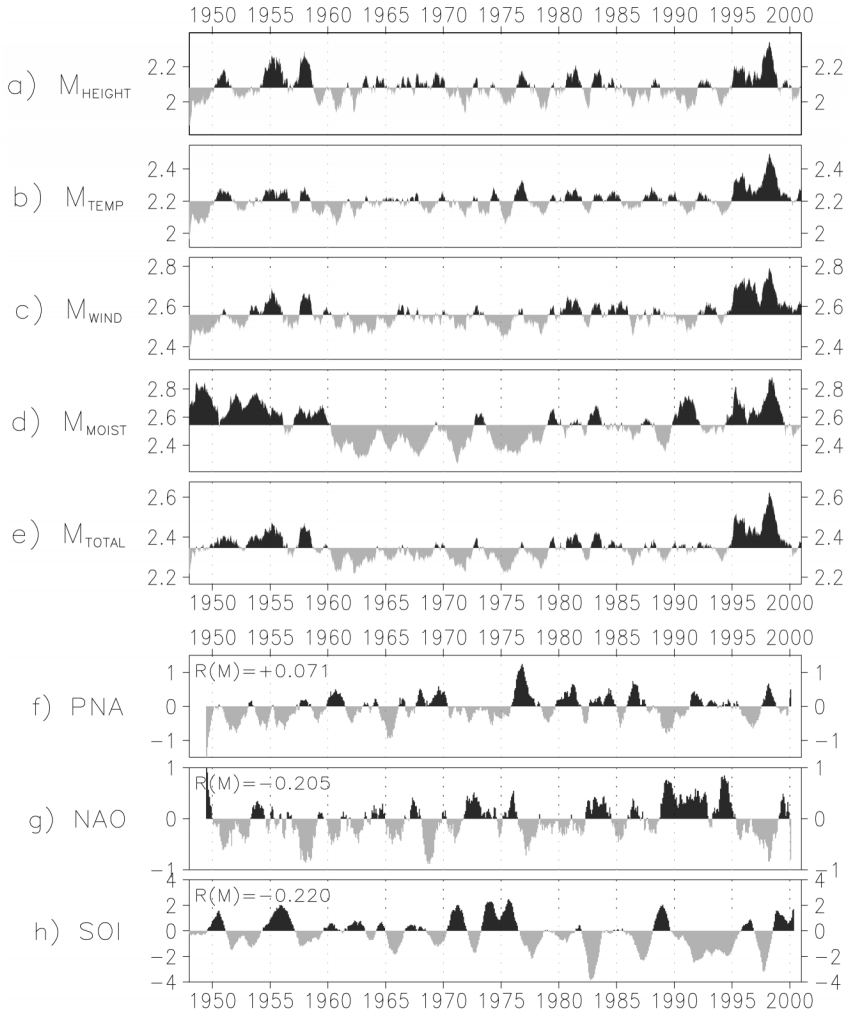

FIG. 7. The 53-yr distribution of anomaly magnitude for each of the four components of M_{TOTAL}: (a) M_{HEIGHT}, (b) M_{TEMP}, (c) M_{WIND}, and (d) M_{MOIST}. (e) Distribution of M_{TOTAL} itself, which is the average of the four previous components. Climate indices: (e) Pacific–North American index (PNA), (f) North Atlantic oscillation (NAO), and (g) Southern Oscillation index (SOI). The R values printed on each panel are calculations of the correlation between M_{TOTAL} and each climate index. A 1-yr running mean smoother has been applied to each time series to remove the annual cycle in each.

the SOI, NAO, and PNA time series, correlations with M_{TOTAL} did not improve significantly and, in most, cases, decreased. Therefore, while the NAO and SOI do modulate the daily extreme activity in eastern North America, the modulation is minimal compared to the natural atmospheric variability on shorter (synoptic) timescales.

Therefore, we are left with the finding that 90%–95% of the observed daily M_{TOTAL} variability across eastern North America cannot be explained by the PNA, NAO, or SOI. This represents a significant result, since several media reports have argued that ENSO in particular did contribute significantly to the apparent increase in severe weather across North American during the late 1990s. However, the analysis performed in Fig. 7. examines the complete cycle of activity for a 53-yr period and thus represents a more robust analysis than the examination of a few individual events. The correlation in Fig. 7h states that, as measured by M_{TOTAL}, synoptic periods of both extreme activity and extreme inactivity are equally as likely to occur during periods of El Niño as they are during periods of La Niña. The natural synoptic-scale variability, chaotic nature of the atmosphere, and the scale mismatch between the long-term ENSO and the shorter-term synoptic-scale M_{TOTAL} measurement are possible reasons for why 90%–95% of the variability in Fig. 7e cannot be explained by long-term climate indices.

In the first five panels of Fig. 7, a dramatic increase in the anomaly magnitudes is observed late in 1994 or early in 1995. Since the data assimilation approach used in the generation of the NCEP reanalysis dataset is a consistent one, such an increase cannot be explained as

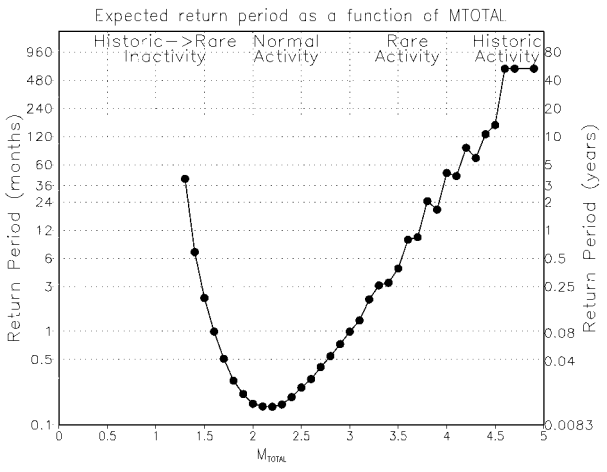

FIG. 8. Expected return period as a function of M_{TOTAL}. Note that the vertical scale is logarithmic. For the period 1948–2000, each 12-h M_{TOTAL} value was binned using a bin width of 0.1 standard deviation. The frequency of occurrence over the 53-yr period was used to arrive at an expected return period. Titles at the top of the figure illustrate the qualitative relative comparison of event frequency.

a methodology change. However, there was a dramatic increase in the availability of satellite-derived measurements in the 1990s. Such an abrupt sustained increase in anomaly magnitudes may be explained by the sudden inclusion of this additional data source. The impact of this additional dataset could be determined by performing the reanalysis without the inclusion of satellite-derived data, a task beyond the scope of this paper. While there was a simultaneous change in the NAO index at that time (Fig. 7), it is hard to argue that a change in the long-wave hemispheric pattern was solely responsible for the M_{TOTAL} jump since many previous jumps in NAO in prior decades were not associated with similar large swings in M_{TOTAL} (Fig. 7).

3) RETURN PERIODS

Given the extent of the database (over 30 000 12-h periods during 53 yr), the expected return periods associated with an M_{TOTAL} of a given magnitude can be approximated (Fig. 8). A bin width of 0.1 standard deviation for each 12-h M_{TOTAL} was used. For simplicity, in this analysis *all* non–tropical cyclone 12-h periods are included; consequently, the issue of data redundancy (and event double counting) is necessarily present and not easily resolved given the continuum of synoptic-scale system evolution. The most common (shortest return period) single M_{TOTAL} value is 2.2 standard deviations. Thus, at any given time we are most likely to find an M_{TOTAL} of 2.2 standard deviations from average across the domain. As M_{TOTAL} decreases, the return period increases very rapidly. An M_{TOTAL} of 1.3 standard deviations represents the *least active weather* found in the dataset with a return period of over 4 yr. An M_{TOTAL} of less than 1.3 standard deviations has never been observed in the 53-yr period. *It is difficult to produce a pattern that supports ''near average'' conditions simultaneously everywhere in the domain* ($M_{\text{TOTAL}} < 1$).

Similarly, as the M_{TOTAL} increases beyond 2.2 standard deviations, the return period increases (Fig. 8). An M_{TOTAL} of 3 standard deviations is observed approximately every month, 4 standard deviations every 4–5 yr, and 4.5 standard deviations every 15 yr (only three times in this dataset period; see Table 2). We can well represent the return period (Fig. 8) as a function of M_{TOTAL} using two piecewise curves (not shown). Extrapolation of the function gives a return period of 80 yr for an M_{TOTAL} of 5 standard deviations and over 400 yr for an M_{TOTAL} of 5.5 standard deviations (both M_{TOTAL} values as yet unobserved in this dataset). A once-a-millennium event would be an M_{TOTAL} of 5.75 standard deviations. All these extrapolations assume that the climate defined by μ, σ in (1) does not change. The distribution shown in Fig. 8 also can be well represented by a gamma function distribution (not shown).

4. Application of rankings to forecast events

This analysis provides the reader with an objective historical context for synoptic-scale events. The utility of this analysis is further enhanced if these rankings can be compared to future events, as forecast by numerical models. Accordingly, the National Weather Service in State College, Pennsylvania, is producing real-time forecasted anomaly fields based upon the Eta, Aviation (AVN), Pennsylvania State University–National Center for Atmospheric Research fifth-generation Mesoscale Model: and Medium Range Forecast (MRF) ensemble models. These forecast anomaly fields show the forecast evolution of anomaly magnitude (similar to the analyses in Figs. 3 and 4) out to 15 days in the future. Further, the MRF-forecasted values of M_{TEMP}, M_{HEIGHT}, M_{WIND}, M_{MOIST}, and M_{TOTAL} are made available out to 7 days in the future (example shown in Fig. 9).

One important caveat that should be stressed is that of grid resolution. While the climatology was developed using 2.5° resolution fields, mesoscale model output is of much higher resolution and able to resolve stronger gradients, extrema, and anomaly magnitudes. Consequently, anomaly fields derived from model output have a significant grid resolution dependence. The authors have found from experience that the high-resolution Eta, MM5, and AVN analyses produce maximum anomaly magnitudes 0.5 to 1 standard deviation larger than the 2.5° reanalysis produce for the same event in the post-analysis. Such differences occur most often for the wind and moisture calculations, where grid resolution has the largest impact. These caveats must be taken into account when examining the forecast anomaly fields available online (cited above). Acknowledging this issue, the forecast time series of M_{TEMP}, M_{HEIGHT}, M_{WIND}, M_{MOIST}, and M_{TOTAL} (Fig. 9) are produced for the 2.5° operational MRF output. This MRF output has a resolution that is

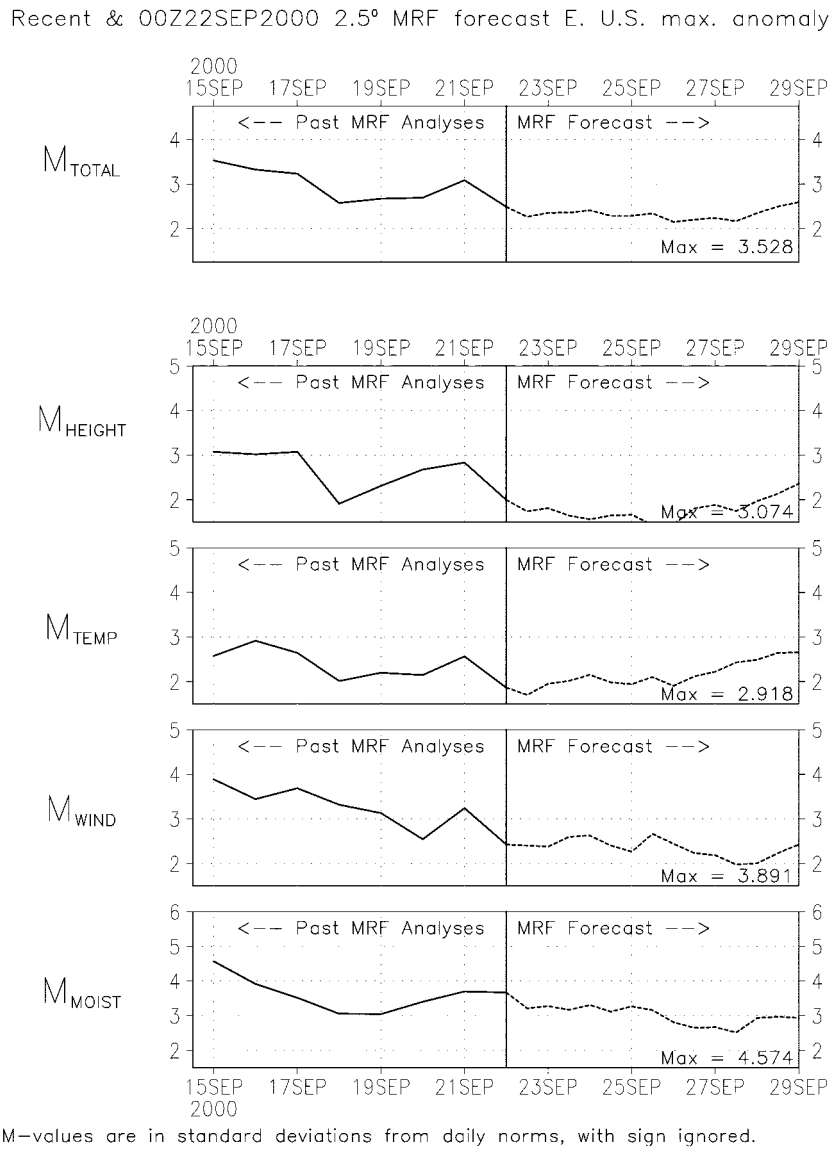

FIG. 9. Example real-time MRF 2.5° resolution forecast of M_{TOTAL} and its components.

consistent with the reanalysis dataset and most reliably compared to the historical rankings shown here.

5. Concluding summary

A method has been proposed for objectively ranking extreme synoptic-scale events over eastern North America by comparing gridded NCEP reanalyses to local climatological means and variability. The maximum full-troposphere departures from climatology for height, temperature, wind, and moisture fields (M_{HEIGHT}, M_{TEMP}, M_{WIND}, M_{MOIST}, respectively) are averaged to produce an objective ranking (M_{TOTAL}). This method successfully identifies and ranks rare or extreme synoptic-scale events. An event having an M_{TOTAL} of 2, 3, 4, or 4.5 standard deviations from average is said to be meteorologically significant, unusual, rare, or extreme, respectively. An M_{TOTAL} of 4.6 or greater (historic) has been observed only three times in the 53-yr period; an M_{TOTAL} of 5 has not been observed since the start of the reanalysis project (1948).

While the state of the atmosphere required to produce these events is unusual (extremely large amplitude longwave troughs at low latitudes, occasionally with cutoff cyclones), the resulting weather observed from these major climatological anomalies varies considerably depending on the time of year and the temperature of the lower atmosphere with respect to freezing. Thus, the method employed here cannot be used to identify the storms that most greatly impacted the population. Accordingly, that was not the intent of the paper. The method does, however, provide a way to objectively compare

anomalous events to determine the rarity of the event, minimizing the biases of land-based observational network density, population density, elevation, and time of year.

We must acknowledge that the decreased observations over oceanic areas produce a land versus ocean anomaly representation bias that cannot be removed by the current approach. However, by using the reanalysis dataset (which includes satellite-derived measurements of wind, temperature, and moisture over the otherwise data-sparse oceanic areas), a significant effort was made to reduce the magnitude of this bias. Finally, the temporally changing density of data availability must be remembered when comparing analyzed anomalies today to those prior to the introduction of moored buoys (1970s) and satellite-derived products (1990s).

The temporal distributions of rare meteorological events were examined. Rare events are far more likely in the late fall through early spring, when baroclinic instability and a concurrent meridional jet stream allow for large departures from climatological averages. However, the NAO index appears to have only a marginal correlation to the observed frequency of M_{TOTAL} ($R = -0.21$). The SOI index has a similar marginal correlation ($R = -0.22$). Such low correlations suggest that these climate measurements describe less than 5% of the observed variability in M_{TOTAL}, leaving 90%–95% of the observed variability unexplained using the conventional climate indices. The M_{TOTAL} value gives a measurement of departure from climatology on the synoptic scale, while climate indices such as ENSO, PNA, and NAO give measurements of planetary wave scale departures from climatology. The planetary-scale wave pattern dictated by ENSO, PNA, and NAO may modulate slightly the occurrence of large M_{TOTAL} events but does not cause or prevent them from occurring.

There do appear to be long-term trends in the frequency of extreme events. The 1950s represent a decade when monthly top 10 events were more frequent than average, with the 1960s and 1970s being decades of relative inactivity. The 1980s and 1990s, however, were two decades of dramatic increase in frequency of monthly top 10 events. Although the changing data density over the 53-yr period introduces uncertainty into these decadal trends, the increased activity during the 1950s and dramatically decreased activity during the 1960s suggests that the decadal trends are likely a real atmospheric cycle and not a consequence of data density.

As future anomalous events occur, the rankings will be updated using the monthly updated reanalyses fields provided by the National Oceanic and Atmospheric Administration/Cooperative Institute for Research in Environmental Sciences (NOAA/CIRES) through the Climate Diagnostics Center (CDC). Updates to the rankings shown in Tables 2–4 will be made available online (http://eyewall.met.psu.edu.). Further, real-time forecast fields from the NCEP Aviation, MRF, and Eta operational models and the local run of the MM5 model are being analyzed using the method shown here. Daily forecast M_{TOTAL} time series are also produced. This enables the user to determine analogs and reference magnitudes for upcoming events using the monthly and all-time rankings provided.

6. Future research

Future research will include evaluating operational model output to help forecasters identify potentially significant or historic weather events. Forecast products will be produced to help evaluate weather events by weather type using the climatological fields and those from operational numerical models and ensembles of these models. If these data prove useful, they could eventually be used in human forecaster and artificial intelligence applications to help assess the risks for flooding, damaging winds, record heat or cold, or record precipitation. Further, future verification methods based upon climatological departures may provide for a more stringent method of verification of events.

Finally, through the rankings provided here we hope that many previously unknown—yet interesting and unusual—synoptic-scale events will be studied. Despite their unusual climatological aspects and meteorological significance, there are a great many cases in Tables 2–4 for which a reference could not be found outside *Storm Data.* As a consequence of those potential case studies and comparisons, a more complete literature on the range of extreme weather events would result.

Acknowledgments. The authors gratefully acknowledge the support of the National Weather Service and COMET for supporting this research. In particular, funds were provided by the University Corporation for Atmospheric Research (UCAR) Subaward UCAR S00-24229. We would like to thank NCEP, NOAA/CIRES, and the CDC for providing the reanalyses grids for the 53-yr period, including the monthly updated fields via the Internet. Further, we are indebted to the Center for Ocean–Land–Atmosphere Studies at the University of Maryland for the use of the GrADS software package. This research was greatly aided by stimulating conversations with George Bryan, Paul Knight, Walt Drag, Lance Bosart, Jenni Evans, and Mike Fritsch. We would like to also thank Paul Head, John LaCorte, and Kevin Fitzgerald of the National Weather Service Office in State College, Pennsylvania, for their investigation of past events. Finally, we greatly appreciate the constructive feedback provided by Gary Carter and Joshua Watson of National Weather Service Eastern Region, John Gyakum, and two anonymous reviewers.

REFERENCES

Abraham, J., K. Macdonald, and P. Joe, 1991: The interaction of Hurricane Hugo with the mid-latitude westerlies. Preprints, *19th Conf. on Hurricanes and Tropical Meteorology,* Miami, FL, Amer. Meteor. Soc., 124–129.

Anthes, R. A., Y.-H. Kuo, and J. R. Gyakum, 1983: Numerical simulations of a case of explosive marine cyclogenesis. *Mon. Wea. Rev.,* **111,** 1174–1188.

Bosart, L. F., and D. B. Dean, 1991: The Agnes rainstorm of June 1972: Surface feature evolution culminating in inland storm redevelopment. *Wea. Forecasting,* **6,** 515–537.

Bristor, C. L., 1951: The great storm of November, 1950. *Weatherwise,* **4,** 10–16.

Cardone, V. J., R. E. Jensen, D. T. Resio, V. R. Swail, and A. T. Cox, 1996: Evaluation of contemporary ocean wave models in rare extreme events: ''Halloween storm'' of October 1991 and the ''storm of the century'' of March 1993. *J. Atmos. Oceanic Technol.,* **13,** 198–230.

DeGaetano, A. T., 2000: Climatic perspective and impacts of the 1998 northern New York and New England ice storm. *Bull. Amer. Meteor. Soc.,* **81,** 237–254.

Dickinson, M. J., L. F. Bosart, W. E. Bracken, G. J. Hakim, D. M. Schultz, M. A. Bedrick, and K. R. Tyle, 1997: The March 1993 superstorm cyclogenesis: Incipient phase synoptic-and convective-scale flow interaction and model performance. *Mon. Wea. Rev.,* **125,** 3041–3072.

DiMego, G. J., and L. F. Bosart, 1982a: The transformation of Tropical Storm Agnes into an extratropical cyclone. Part I: The observed fields and vertical motion computations. *Mon. Wea. Rev.,* **110,** 385–411.

——, and ——, 1982b: The transformation of Tropical Storm Agnes into an extratropical cyclone. Part II: Moisture, vorticity, and kinetic energy budgets. *Mon. Wea. Rev.,* **110,** 412–433.

Fujita, T. T., 1981: Tornadoes and downbursts in the context of generalized planetary scales. *J. Atmos. Sci.,* **38,** 1511–1534.

Gaza, B., and L. F. Bosart, 1990: Trough merger characteristics over North America. *Wea. Forecasting,* **5,** 314–331.

Grumm, R. H., and D. Nicosia, 1997: WSR-88D observations of mesoscale precipitation bands over Pennsylvania. *Natl. Wea. Dig.,* **21,** 10–23.

Gyakum, J. R., 1983a: On the evolution of the *QE II* storm. Part I: Synoptic aspects. *Mon. Wea. Rev.,* **111,** 1137–1155.

——, 1983b: On the evolution of the *QEII* storm. Part II: Dynamic and thermodynamic structure. *Mon. Wea. Rev.,* **111,** 1156–1173.

——, 1991: Meteorological precursors to the explosive intensification of the *QEII* Storm. *Mon. Wea. Rev.,* **119,** 1105–1131.

Hakim, G. J., L. F. Bosart, and D. Keyser, 1995: The Ohio Valley wave-merger cyclogenesis event of 25–26 January 1978. Part I: Multiscale case study. *Mon. Wea. Rev.,* **123,** 2663–2692.

——, D. Keyser, and L. F. Bosart, 1996: The Ohio Valley wave-merger cyclogenesis event of 25–26 January 1978. Part II: Diagnosis using quasigeostrophic potential vorticity inversion. *Mon. Wea. Rev.,* **124,** 2176–2205.

Hoskins, B., and P. J. Valdes, 1990: On the existence of storm-tracks. *J. Atmos. Sci.,* **47,** 1854–1864.

Jarvinen, B. R., C. J. Neumann, and M. A. S. Davis, 1984: A tropical cyclone data tape for the North Atlantic basin, 1886–1983: Contents, limitations, and uses. NOAA Tech. Memo. NWS NHC 22, 21 pp.

Junger, S., 1997: *The Perfect Storm.* Harper, 302 pp.

Kalnay, E., and Coauthors, 1996: The NCEP/NCAR 40-Year Reanalysis Project. *Bull. Amer. Meteor. Soc.,* **77,** 437–471.

Knox, J. L., 1955: The storm ''Hazel,'' synoptic resume of its development as it approached southern Ontario. *Bull. Amer. Meteor. Soc.,* **36,** 239–246.

Kocin, P. J., and L. W. Uccellini, 1990: *Snowstorms along the Northeastern Coast of the United States: 1955 to 1985. Meteor. Monogr.,* No. 44, Amer. Meteor. Soc., 280 pp.

——, P. N. Schumacher, R. F. Morales Jr., and L. W. Uccellini, 1995: Overview of the 12–14 March 1993 superstorm. *Bull. Amer. Meteor. Soc.,* **76,** 165–182.

Leathers, D. J., D. R. Kluck, and S. Kroczynski, 1998: The severe flooding event of January 1996 across north-central Pennsylvania. *Bull. Amer. Meteor. Soc.,* **79,** 785–797.

Ludlum, D. M., 1951: Winter strikes early in 1951. *Weatherwise,* **4,** 131–141.

——, 1952: An intense November storm. *Weatherwise,* **6,** 18–19.

——, 1956: The Great Atlantic Low. *Weatherwise,* **9,** 64–65.

——, 1958a: Winter 1957–1958: A divided nation. *Weatherwise,* **11,** 67–73.

——, 1958b: Eve of spring snowstorm. *Weatherwise,* **11,** 109.

NOAA, 1959–2000: *Storm Data.* Vols. 1–42. [Available from NCDC, 151 Patton Ave., Asheville, NC 28801-S001.]

Palmén, E., 1958: Vertical circulation and release of kinetic energy during the development of Hurricane Hazel into an extratropical storm. *Tellus,* **10,** 1–23.

Palmer, W. C., 1965: Meteorological drought. Research Paper 45, U.S. Department of Commerce Weather Bureau, Washington, DC, 58 pp.

Pearce, M. L., 1997: Non-classic and weakly forced convective events: A forecasting challenge for the dominant form of severe weather in the Mid Atlantic region of the United States. M.S. thesis, Dept. of Meteorology, The Pennsylvania State University, 106 pp. [Available from Dept. of Meteorology, The Pennsylvania State University, 503 Walker Building, University Park, PA 16802.]

Ruscher, P. H., and T. P. Condo, 1996a: Development of a rapidly deepening extratropical cyclone over land. Part I: Kinematic aspects. *Mon. Wea. Rev.,* **124,** 1609–1632.

——, and ——, 1996b: Development of a rapidly deepening extratropical cyclone over land. Part II: Thermodynamic aspects and the role of frontogenesis. *Mon. Wea. Rev.,* **124,** 1633–1647.

Sanders, F., and J. R. Gyakum, 1980: Synoptic-dynamic climatology of the ''bomb.'' *Mon. Wea. Rev.,* **108,** 1589–1606.

Schwartz, G., 1977: The day it snowed in Miami. *Weatherwise,* **30,** 50.

Simpson, R. H., 1974: The hurricane disaster-potential scale. *Weatherwise,* **27,** 169.

Treidl, R. A., 1959: The great Midwinter storm of 20–22 January 1959. *Weatherwise,* **12,** 45–47.

Uccellini, L. W., 1986: The possible influence of upstream upper-level baroclinic processes on the development of the *QEII* storm. *Mon. Wea. Rev.,* **114,** 1019–1027.

van Loon, H., and J. C. Rogers, 1978: The seesaw in winter temperatures between Greenland and northern Europe. Part I: General description. *Mon. Wea. Rev.,* **106,** 296–310.

Watson, B., 1993: New respect for nor'easters. *Weatherwise,* **46,** 18–23.